Earth Sciences
2020; 9(5): 148-163
http://www.sciencepublishinggroup.com/j/earth
doi: 10.11648/j.earth.20200905.12
ISSN: 2328-5974 (Print); ISSN: 2328-5982 (Online)

Predictive Mapping of the Mineral Potential Using Geophysical and Remote Sensing Datasets in Parts of Federal Capital Territory, Abuja, North-Central Nigeria

Ejepu Jude Steven[1, *], Abdullahi Suleiman[1], Abdulfatai Asema Ibrahim[1], Umar Mohammed Umar[2]

[1]Department of Geology, School of Physical Sciences, Federal University of Technology, Minna, Nigeria

[2]Department of Geology and Mining, Faculty of Applied Sciences and Technology, Ibrahim Badamasi Babangida University, Lapai, Nigeria

Email address:
ejepu.jude@futminna.edu.ng (E. J. Steven)

[*]Corresponding author

To cite this article:
Ejepu Jude Steven, Abdullahi Suleiman, Abdulfatai Asema Ibrahim, Umar Mohammed Umar. Predictive Mapping of the Mineral Potential Using Geophysical and Remote Sensing Datasets in Parts of Federal Capital Territory, Abuja, North-Central Nigeria. *Earth Sciences*. Vol. 9, No. 5, 2020, pp. 148-163. doi: 10.11648/j.earth.20200905.12

Received: July 23, 2020; **Accepted**: August 22, 2020; **Published**: September 17, 2020

Abstract: Mineral Prospectivity Mapping (MPM) is a multi-step process that ranks a promising target area for more exploration. This is achieved by integrating multiple geoscience datasets using mathematical tools to determine spatial relationships with known mineral occurrences in a GIS environment to produce mineral prospectivity map. The study area lies within Latitudes 9° 00′ N to 9° 15′ N and 6° 45′ to 7° 00′ E and is underlain by rocks belonging to the Basement Complex of Nigeria which include migmatitc gneiss, schist, granite and alluvium. The datasets used in this study consist of aeromagnetic, aeroradiometric, structural, satellite remote sensing and geological datasets. Published geologic map of the Sheet 185 Paiko SE was used to extract lithologic and structural information. Landsat images were used to delineate hydroxyl and iron-oxide alterations to identify linear structures and prospective zones at regional scales. ASTER images were used to extract mineral indices of the OH-bearing minerals including alunite, kaolinite, muscovite and montmorillonite to separate mineralized parts of the alteration zones. Aeromagnetic data were interpreted and derivative maps of First Vertical Derivative, Tilt derivative and Analytic signal were used to map magnetic lineaments and other structural attributes while the aeroradiometric dataset was used to map hydrothermally altered zones. These processed datasets were then integrated using Fuzzy Logic modelling to produce a final mineral prospectivity map of the area. The result of the model accurately predicted known deposits and highlighted areas where further detailed exploration may be conducted.

Keywords: Geophysical Methods, Mineral Exploration, Fuzzy Logic Models, Geographic Information Systems, Remote Sensing

1. Introduction

Modern mineral exploration efforts in recent times have adopted the integration of different datasets from various sources and surveys. Therefore, an important phase in mineral exploration should involve the collection, analysis, interpretation and integration of remotely sensed, geological, geophysical and geochemical datasets. This is done in order to map prospective areas for a more detailed investigation. Mineral Prospectivity Mapping (MPM) is basically classified into empirical (data driven) and conceptual (knowledge driven) methods [1-2]. In the data driven method, known mineral deposits are used as 'training points' for examining spatial relationships between the known deposits and geological, geochemical and geophysical features of interest. The identified relationships between input data and training points are quantified and used to establish the importance of each evidence map and subsequently integrated into a single mineral prospectivity map. Examples of the empirical methods used are weights of evidence, logistic regression and neural networks.

However, in the conceptual (knowledge driven) method, conceptualisation of knowledge about the mineral deposit is devised in order to create a mappable criterion. These include

making inferences about threshold values in criteria that control the mineralisation style. The areas that satisfy most of these criteria are delineated as being the most prospective. These methods are subjective based on the geologist's input and the proposed exploration model. By selecting a conceptual method, one can benefit from the expertise of the geologists during the modelling process exceeding the capabilities of pure statistics. The methods belonging to this branch include Boolean logic, index overlay (binary or multi-class maps), the Dempster-Shafer belief theory, and fuzzy logic overlay.

Hence, the choice of methods to be applied are often made based on the availability of disparate datasets and modelling goals [3]. The fuzzy logic method has been recently widely implemented for the data integration and MPM purposes [4-7]. The fuzzy method enables evidence maps to be combined into a series of steps regarded as an inference net (flowchart), instead of combining them in a single operation. The inference net is a simulation of the logical process defined by a specialist [8].

In this study, fuzzy logic technique was selected due to its potential accurately delineate hydrothermal and structural controlled mineralization in the study area located within the Federal Capital Territory (FCT) Abuja, North-Central Nigeria. Several studies have shown the feasibility of multispectral remote sensing for mapping the hydrothermally altered rock [2, 9, 10]. Spectral discrimination of potential areas of gold mineralization (hydrothermal alteration zones) is a common application of remote sensing data analysis [11]. Here, Advanced Spaceborne Thermal Emission and Reflection Radiometer (ASTER) data was processed and analysed for gold mineralization mapping in the study area.

Structural controls and the distribution pattern of hydrothermal alteration zones have been used as indicators of mineralized zones within the study area. Hence, a GIS-based spatial analysis was applied to evaluate mineral potential in the study area by using mineral favourability maps in order to define areas for detailed investigations.

2. Study Area

2.1. Geology of the Area

The study area forms part of reworked West African Craton and underlies about 60% of Nigeria's land mass [12]. The Basement Complex has been described as a heterogeneous assemblage, which includes migmatites, gneisses, schists and a series of basic to ultrabasic metamorphosed rocks. Pan African Granites and other minor intrusions such as pegmatite and Aplites dykes and quartz veins have intruded these rocks (Figure 1) [13].

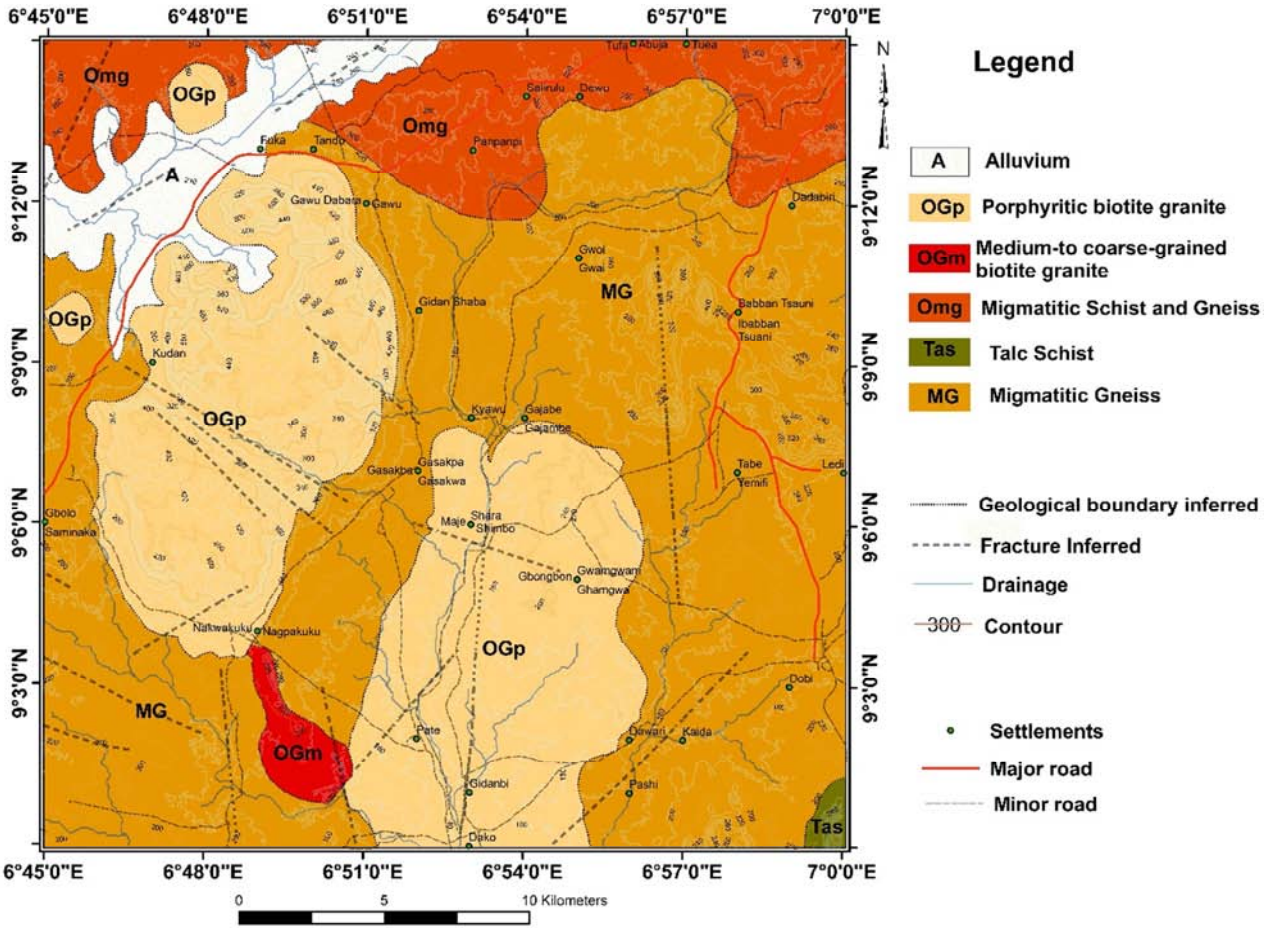

Figure 1. *Geologic map of the area. Some fault lines are digitized from published geologic map. (Source: Nigerian Geological Survey Agency (NGSA), 2009).*

All these rocks were affected and deformed by the Pan-African thermotectonic event. Detailed reports of the lithological description, age, history, structure and geochemistry of the Basement Complex of Nigeria are given in [13-18].

2.1.1. The Metasediments

The Metasedimentary/Metavolcanic series consist of phyllites, schists, amphibolites, quartzites and serpentinites. The series comprises low grade, metasediment-dominated belts trending north-south and considered to be Upper Proterozoic super crustal rocks that have been infolded into the migmatite-gneiss complex. The lithological differences include fine to coarse grained clastics, politic schists, phyllites, carbonate rocks (marble and dolomitic marbles) and mafic metavolcanics (amphibolites). The existence of many basins of deposition has been suggested by [19, 20]. It is considered as a relict of a single supracrustal cover and fault-controlled rift-like structures [14, 21, 22].

2.1.2. The Migmatite – Gneiss Complex

The Migmatite-Gneiss complex comprises the most widespread group of rocks and is it considered as the Basement Complex *sensu stricto* [13, 18]. It comprises migmatites, orthogneisses, paragneisses, quartzites, calc-silicate rocks, biotite-hornblende schist and amphibolites. On account of petrography, the Pan African orogeny culminated in the recrystallisation of many of the constituent minerals of the Migmatite-Gneiss Complex by partial melting with most of the rocks showing medium to high grade amphibolites facies metamorphism. The Migmatite-Gneiss Complex displays ages varying from Pan African to Eburnean with three main geological phenomena recorded. The first at 2,500 Ma, involved in initiation of crust forming process and of crustal growth by sedimentation and orogeny; the second event was the Eburnean; 2,000 + 200 Ma, marked by the granite gneisses, which structurally obliterated the older rocks and reset the geochronological clock to give rise to granite gneisses, migmatites and other similar lithological units [23].

2.2. Structural Geology of the Region

The structural elements in Nigerian Basement include joints, fractures, lineations and folds (minor and major). The E-W trending structures are deep seated in origin and ancient in age and resulted from various thermotectonic deformational episodes mostly of the Eburnean and Pan-African Orogeny [24-26]. Dominant surface structural trend in the basement is essentially NE-SW trends comparable with the tectonic grains of the schist belt. The NW-SE and E-W trends are locally dominant. Several sets of fractures having NW-SE, NNW-SSE, NNE-SSW and NE-SW directions were produced by transcurrent movement and shearing were also observed in the study area [27].

3. Materials and Methods

In mineral exploration studies, method selection and tools to be applied are often dependent upon the mode of occurrence and formation of targeted mineral deposits [28]. This research has its target on gold occurrences, which occur in fractures and are related to shear zones. Therefore, the best surface indications for these features are structural controls and hydrothermal alterations. These features are usually expressed as lineaments and lithological contrasts, respectively.

3.1. Satellite Imagery

3.1.1. Landsat 8 OLI

The satellite imagery used was clipped from the Landsat 8 scene LC81890542018016LGN00, from 20 January, 2018 from the earthexplorer.usgs.gov website, collected by sensors OLI (Operational Land Imager) and TIRS (Thermal Infrared Sensor). Landsat 8 band specifications are presented in Table 1. This scene was chosen due to its near perfect quality (9/9), the virtually non-existent cloud coverage (0.98/100) and due to the relatively low solar elevation (49.55°).

Table 1. *Landsat band specifications. Source: [29]*

Sensor	Band	Spectral Resolution (μm)	Spatial resolution (m)
OLI	Band 1-Coastal	0.435-0.451	30
	Band 2-Blue	0.452-0.512	30
	Band 3-Green	0.533-0.590	30
	Band 4-Red	0.636-0.673	30
	Band 5-NIR	0.851-0.879	30
	Band 6-SWIR-1	1.566-1.651	30
	Band 7-SWIR-2	2.107-2.294	30
	Band 8-Pan	0.503-0.676	15
	Band 9-Cirrus	1.363-1.384	30
TIRS	Band 10-TIR-1	10.6-11.19	100
	Band 11-TIR-2	11.50-12.51	100

3.1.2. ASTER

The extent of the study area was clipped from the ASTER Scene AST_L1T_00301282002100954_20150424050755_62951 of 28th of January, 2002 from https://earthdata.nasa.gov/. The scene has solar elevation of 59° and perfect cloud cover cloud cover of 0%. ASTER band specifications are presented in Table 2. It provides higher spatial, spectral, and radiometric resolutions than traditional Landsat data [30]. The ASTER channels are more contiguous in the shortwave infrared region than those of Landsat, yielding increased accuracy in the spectral identification of rocks and minerals [31]. More spectral bands provide a better understanding of the geology and soils of the earth surface. This is what makes ASTER data superior over other sensors for lithological mapping [32-35].

The digital pre-processing, processing and preliminary lineament mapping of the SRTM, Landsat 8 and ASTER data were executed using ENVI software. Atmospheric correction

of Landsat 8 OLI and ASTER images were performed using the FLAASH module of ENVI software. Spectral resampling has been used to downscale the spatial resolution of the SWIR bands of the ASTER data to 15 m.

Table 2. *ASTER band specifications.*

Sensor	Band No.	Spectral Resolution (μm)	Spatial resolution (m)
VNIR	1	0.52-0.60	15
	2	0.63-0.69	15
	3N	0.78-0.86	15
	3B	0.78-0.86	15
SWIR	4	1.60-1.70	30
	5	2.145-2.185	30
	6	2.185-2.225	30
	7	2.235-2.285	30
	8	2.295-2.365	30
	9	2.360-2.430	30
TIR	10	8.125-8.475	90
	11	8.475-8.825	90
	12	8.925-9.275	90
	13	10.25-10.95	90
	14	10.95-11.65	90

3.1.3. SRTM DEM

The National Imagery and Mapping Agency (NIMA), National Aeronautics and Space Administration (NASA) and German Aerospace Centre (DLR) collaborated to launch the SRTM Mission on February 11, 2000 with the primary objective of acquiring elevation data on a near-global scale and generate the most complete high-resolution digital topographic database of the Earth. Using the Space borne Imaging Radar-C and X-Band Synthetic Aperture Radar (SIR-C and X-SAR) hardware, SRTM collected data that were used to generate a digital elevation model with data points spaced every 1 arc second of latitude and longitude (approximately 30 metres at the equator). The absolute horizontal and vertical accuracy is better than 20 metres and 16 metres, respectively. SRTM uses radar interferometry. The 30 m SRTM data was downloaded from http://dwtkns.com/srtm30m/. This site is an interface that attempts to ease the pain of downloading 30-meter resolution elevation data from the Shuttle Radar Topography Mission website.

High-pass convolution filters (directional edge) from a Kernel 3 x 3 matrix were applied to the SRTM DEM image to emphasize the structures parallel to the direction of each filter (Drury, 2001). The directional filters were applied for the azimuths 0°, 45°, 90°, 135°, 180°, 225°, 270° and 315° for a comprehensive cover of the area using the ENVI software (Exelis Visual Information Solutions, Boulder, CO, USA)

3.1.4. Aero Geophysical Data

The aeromagnetic inversion method is based on processing of the total field magnetic anomaly. Total magnetization is the rock property associated to its magnetic anomaly and geologic origin [35] in the direction of the earth's field. The total field aeromagnetic anomalies include both induced and remnant magnetic fields. This is a reflection of variations in the amount and type of subsurface magnetic minerals, hence, important for geophysical prospecting of mineral resources. The aeromagnetic data was obtained from Nigeria Geological Survey Agency (NGSA). The data were captured for NGSA from 2005 to 2010 by Fugro Airborne Surveys as part of nationwide airborne geophysical surveys. The data were acquired along a series of NE–SW profiles with a flight line spacing of 500 m and terrain clearance of 80 m. For this study one half degree sheet covering the study area was utilised. The total magnetic intensity field was International Geomagnetic Reference Field [36] corrected and a super-regional field of 32,000 nT was deducted from the raw data. Oasis montaj software was used to grid the data at 125 m spatial resolution using the minimum curvature gridding method [37]. Subsequently, it was subjected to Reduction to Magnetic Equator (RTE) and further processing were carried out in order to investigate the presence of buried structures that might be relevant in mineral exploration.

The aeroradiometric data was acquired using a high-sensitivity 256-channel airborne gamma ray spectrometer. The data of the survey was available in the form of total count, Potassium, equivalent Uranium, and equivalent Thorium data in a digital form. Enhancement and interpretation processes was done by using Oasis montaj software.

3.2. Data Processing

3.2.1. Alteration Mapping

The most important mineralogical difference between altered and unaltered rocks is the abundance of alteration minerals such as alunite, montmorillonite and kaolinite in the altered rocks. Furthermore, the difference between mineralized and non-mineralized altered rocks is the presence of abundant secondary iron minerals such as goethite, hematite, limonite and jarosite in association with other alteration minerals. In altered rocks, the change in abundance of any of the above-mentioned alteration minerals would lead to a slight change in the reflectance value that depends on that mineral's spectral characteristics.

3.2.2. Landsat 8 OLI

The following common digital processing techniques were used: Red, Green, Blue (RGB) colour composites, Principal Component Analysis (PCA), directional spatial filters and band ratios. Rationing is a common procedure used for feature enhancements based on the division of every pixel value of one band by the homologous pixels of the other band (Prost, 1983). A ratio is created by dividing brightness values, pixel by pixel, of one band by another so as to enhance spectral differences and suppress illumination differences. Band ratios of Landsat 8 OLI data are used to enhance rock alteration. Ratios exaggerate some subtle differences in spectral response. A false colour composite can then be made in such a way that each ratio band is then assigned one of the three primary colours with the lighter parts (high DN values) of the band contributing more colour to the composite.

In this study, band ratios 4/2, 5/6, and 6/7 (RGB) has been used. This combination is selected for their sensitivity to lithologic variables, and for their lack of statistical redundancy [38]. The ratio of bands 4/2 enhances rocks with an abundance of ferric iron oxide (limonite) responsible for the hydrothermal alteration or the oxidation of Fe-Mg silicates. The ratio of bands 5/6 enhances rocks which are rich in ferrous iron and band ratio 6/7 enhances rocks having Al-OH, such as those clay and sulphate minerals produced from hydrothermal fluids.

3.2.3. ASTER Data

A hybrid method based on the combination of band ratio images and the PCA transformation method of [39] who used the four mineralogical indices proposed by [40] for hydrothermal alteration mapping. The formulae of indices are listed below:

OHI=(band 7/band 6) (band 4/band 6)

KLI=(band 4/band 5) (band 8/band 6)

ALI=(band 7/band 5) (band 7/band 8)

CLI=(band 6/band 8) (band 9/band 8)

where OHI is the index for OH-bearing minerals, KLI is the kaolinite index, ALI is the alunite index, and CLI is the calcite index. Each index was thresholded and then merged spatially to map the alteration zones using the mineralogical indices for each alteration mineral. Results obtained from these indices include feasibility-abundance maps of the OH-bearing minerals including alunite, kaolinite, muscovite and montmorillonite from the SWIR surface reflectance data [40].

An ASTER band ratio image (bands 4/8, 4/2, and 8/9 in RGB respectively) has been created for better separation of the mineralized parts of the alteration zones (Figure 4). The ratio 4/8 was chosen to increase the response of the iron oxides in the altered mineralized rocks. The ratio 4/2 separates altered mineralized rocks from all the other background materials (both altered non-mineralized and the unaltered rocks). Finally, and for better contrast for the resulting image, 8/9 ratio was chosen to make an image for averaged values from all the rock units in the image area.

3.3. Aeromagnetic Data

3.3.1. Vertical, Total Gradient and Tilt Derivatives

First vertical derivative can be applied either in space or frequency domain. It is proposed by [41], using 3D Hilbert transforms in the x and y directions. It is used in this study to supress deeper anomalies while enhancing shallow features with their boundaries so as to make lineaments extraction easier. This is achieved by the vertical derivative amplifying short-wavelengths at the expense of longer ones, therefore making it easier for shallower causative sources to be mapped. Also, the analytic signal (total gradient) can be calculated either in space or frequency domain, producing a maximum directly over discrete bodies as well as their edges. Analytic signal is formed through the combination of the horizontal and vertical gradients of the magnetic anomaly and its amplitude is independent on the magnetisation direction. This filter applied to reveal the anomaly texture and highlight discontinuities also enhance short-wavelength anomalies [42, 43].

The amplitude of the signal peak of analytic signal is directly proportional to the edge of magnetization. Hence source edges are easily determined. The magnetic tilt derivative (TDR) combines all three gradients (X, Y and Z) to produce what is a called a tilt angle. This product highlights very subtle, near surface structures in the dataset where the zero-contour line of the grid is said to represent geology contacts or edges of bodies.

3.3.2. Aeroradiometric Data

Gamma-ray spectrometry (GRS) can be very helpful in mapping surface geology. The method provides estimates of apparent surface concentrations of the most common naturally occurring radioactive elements comprising potassium (K), equivalent uranium (eU), and equivalent thorium (eTh). The use of the method for geological mapping is based on the assumption that absolute and relative concentrations of these radio elements vary measurably and significantly with lithology. The aeroradiometric technique assists considerably in mapping surface structure, lithological units and identification of hydrothermal alteration zones. The radiometric data are gridded to obtain total count, potassium, equivalent thorium and equivalent uranium maps to show the surface distribution of these elements. Also, producing K/eTh ratio map help to map hydrothermally altered zones, since a reduction in eTh and a rise in K is an indicator of alteration environments in an ore deposit [44]. Finally, a ternary map is created by combining the three radioelements concentration in the RGB colours.

3.4. Lineament Extraction

3.4.1. Surface Lineament Extraction

In order to extract lineaments from the remotely sensed datasets, directional spatial filters are applied so as to modify pixel values of the remotely sensed images based on the values of neighbouring pixels using 3X3 kernels allowing for edge enhancement in a particular direction [28, 45, 46]. The main applications of this type of filters include: obtaining sharper and more detailed images, edge enhancement and reducing local illumination effects [47]. Four directional filters depicted in (Table 3) were applied to the Landsat 8 OLI, ASTER and SRTM DEM datasets. All lineaments from various remotely sensed datasets were merged to form a composite surface lineament map of the study area and subsequently plotted as a Rosette diagram. To group these features, the classification used by was adopted, where the N-S and E-W limits comprise a margin of 10º in clockwise and anti-clockwise directions [48].

Table 3. *Directional spatial filters applied to Landsat 8 imagery Richards and Jia, 2006.*

N-S			W-E			NW-SE			NE-SW		
-1	-1	-1	-1	0	1	-1	-1	0	0	-1	-1
0	0	0	-1	0	1	-1	0	1	1	0	-1
1	1	1	-1	0	1	0	1	1	1	1	0

3.4.2. Magnetic Lineament Extraction

Magnetic lineaments were delineated using the CET Grid Analysis plugins included in Oasis montaj software. The CET grid analysis is a new technique developed by Centre for Exploration Targeting (CET), University of Western Australia. It consists of a number of tools that provide automated lineament detection of gridded data, which can be used for first-pass data processing. As explorers often have large volumes of gridded data to interpret, these tools provide a rapid unbiased workflow that reduces the time with which one can interpret gridded data.

The extension is specifically designed for mineral exploration geophysicists and geologists looking for discontinuities within magnetic and gravity data. The CET Grid Analysis provides a step-by-step trend detection menu which offers two different approaches to trend estimation. The first method, *Texture analysis-based image enhancement*, is suitable for analysing regions of subdued magnetic or gravity responses where texture analysis can first enhance the local data contrast. The second method, *Discontinuity structure detection*, is useful in identifying linear discontinuities and edge detection. These methods use a phase-based approach which will ensure that even features lying in low contrast regions will be detected. Edge detection process starts with Lineation Detection, to find edges in magnetic data irrespective of their orientation or contrast with the background. This is followed by Lineation Vectorization to generate trend line estimates from the edge information detected by the phase congruency transform. The phase congruency transform is a contrast-invariant edge detection method based on observing the local spatial frequencies [49, 50].

3.5. Final Fuzzy Integration Procedure

The fuzzy logic method allows weights to be assigned to each evidential layer based upon informed decisions and opinions. The fuzzy-set theory defines a degree of membership in a set represented by a value between 0 and 1. The value of the membership function can be determined by two methods. One method is to calculate according to the membership function curve; the other is to assign values artificially according to geological knowledge. The fuzzy model in mineral prediction consists of two steps: (1) fuzzification of data (2) fuzzy synthesis of fuzzified data. Fuzzy synthesis is executed using the operator. The most basic fuzzy operators are: fuzzy AND, fuzzy OR, fuzzy algebraic product, fuzzy algebraic sum, and fuzzy gamma.

The fuzzy Sum operator highlights the maximum values available for all input criteria. The sum fuzzy operator assumes that the more favourable input is better. The resulting sum is an increasing linear combination function that is based upon the number of criteria entering the analysis. The fuzzy Gamma type is an algebraic product of fuzzy Product and fuzzy Sum, which are both raised to the power of gamma. The generalize function is as follows: $\mu(x)=(\text{FuzzySum})^{\gamma} * (\text{FuzzyProduct})$. The final prospective map was prepared with fuzzy γ=0.9 operator. The fuzzy gamma operator was used to calculate the final prospectivity map in the present study.

4. Results and Discussion

4.1. Alteration Mapping

Hydrothermal deposits develop along faults and fractures. Increased permeability along faults probably controlled the pathways followed by fluids that deposited metals and gangue minerals [51]. Therefore, faults and major fractures are considered as potential localizers for ore deposition. The major faults were delineated from enhanced aeromagnetic data, Landsat 8 OLI, SRTM satellite image and geological map of the study area.

The detection of alteration zones using Landsat 8 OLI images marked by the presence of iron oxides, hydroxyl-bearing minerals and hydrothermal clays was made possible from false colour composite image band ratios of 6/4, 4/2 and 6/7 in red, green and blue [52-56]. Primary colours of red, green and blue are indicative of high ratio value band ratios of 6/4, 4/2 and 6/7 respectively. High band ratio values of two colours are depicted in the pixel as a combination of two colours proportional to their values. High 6/4 values (red) give a high composition of iron oxides (both ferric and ferrous); large 4/2 values (green) represent a large component of ferric oxides associated soils. For example, iron oxide-rich parts of the alteration are considered to be the main target for gold exploration.

Furthermore, high 6/7 values (blue) represent the presence of hydrothermal clays since the band 6 covers the reflectance peak of hydrothermal clays whereas band 7 contains a reflectance trough of the clays. A large 6/4 and 4/2 band ratio values in the same pixel will display as yellow, while high band ratios of 6/4 and 6/7 value in one pixel will be displayed as pink. The largely blue areas in the study area of the band ratio composite map correlates well with areas having high lineament densities. These areas are rich in iron oxide minerals and hydrothermally altered clays (Figure 2). Ferric minerals are found doting around other parts of the study area.

The method for Landsat OLI was adapted also to create the ASTER alteration images (Figure 3). In this case, iron oxides, hydroxyl-bearing minerals and hydrothermal clays were used as false colour composite image band ratios of 4/8, 4/2 and 8/9 in red, green and blue were created. A large 4/8 and 4/2 band ratio values in the same pixel will display as yellow, while high band ratios of 4/2 and 8/9 value in one pixel will be displayed as blue. Mapped mineralogical units related to gold deposits maybe used as an exploration tool in areas around the study area where promising locations are expected. It is to be noted that several field visits were carried out for updated lithological mapping resulting in the production of the geological map that provided useful information for this study.

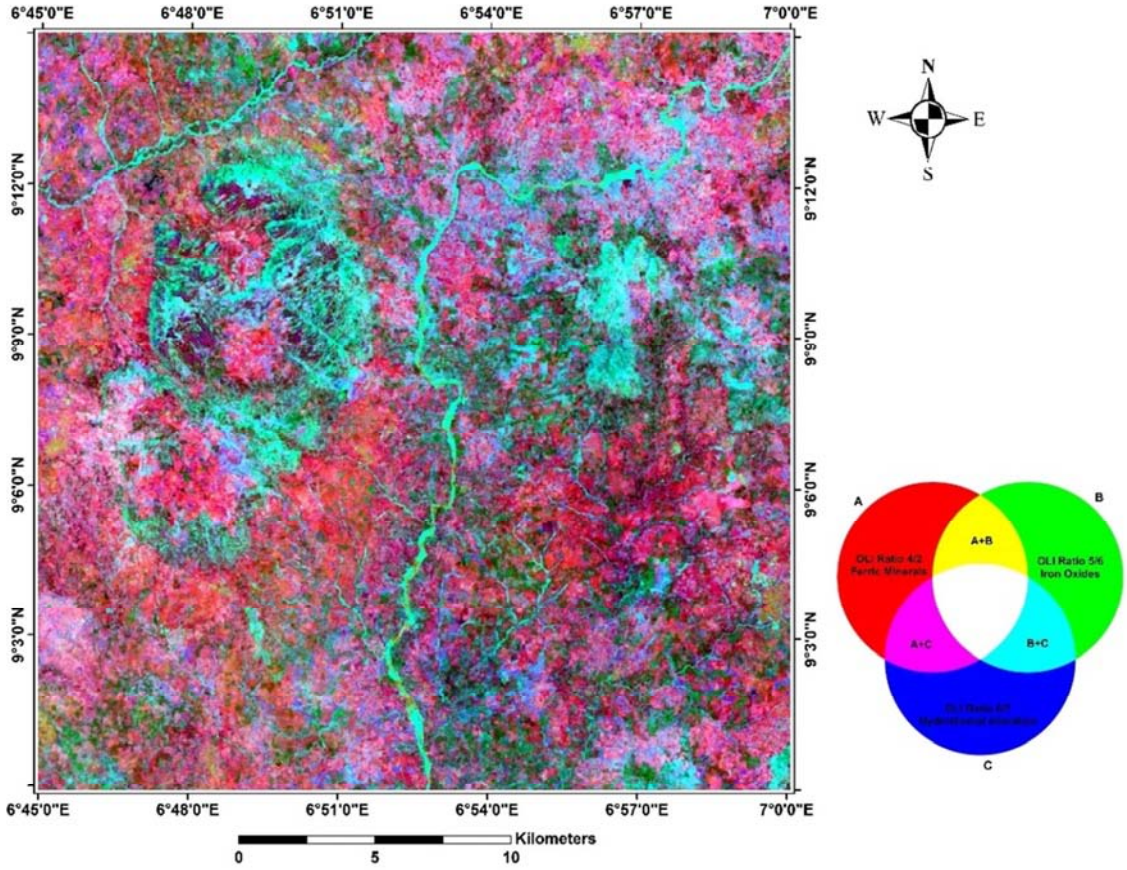

Figure 2. *Landsat False Colour Composite.*

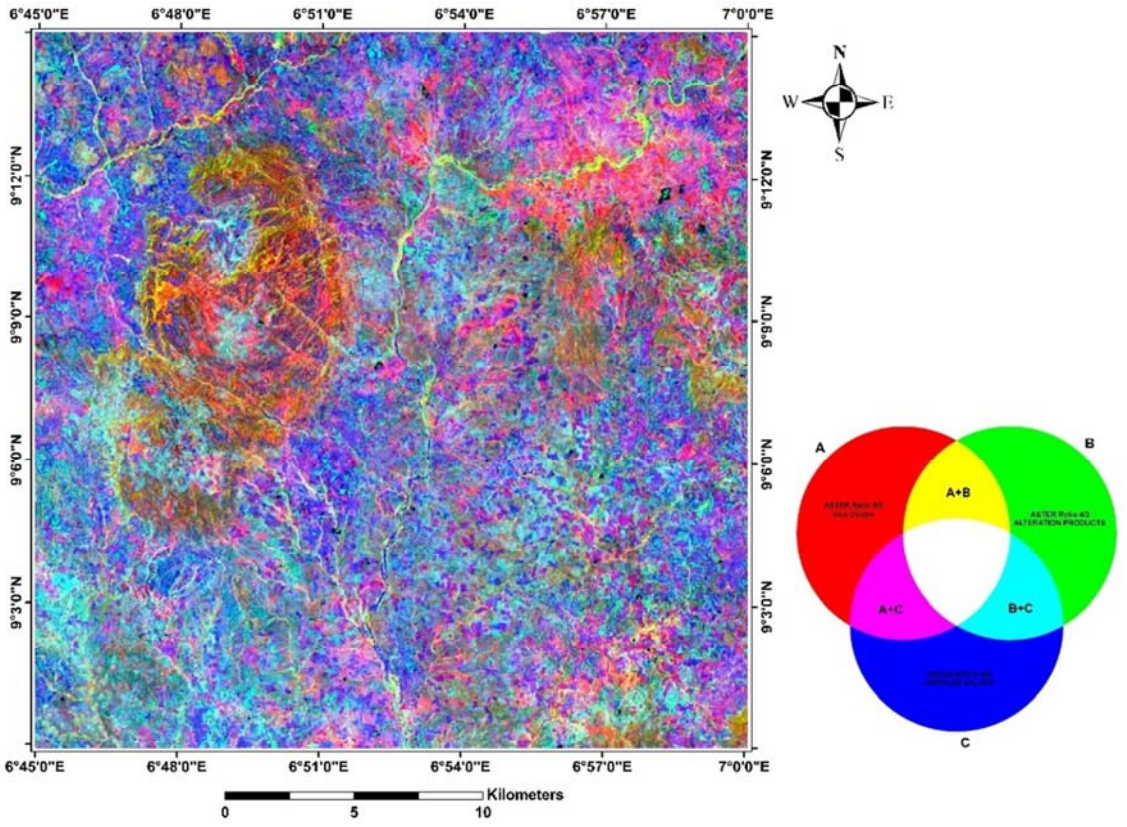

Figure 3. *ASTER False Colour Composite.*

4.2. Aeromagnetic Data Analyses

Residual magnetic anomaly image (Reduced to Equator (RTE) (Figure 4) shows an amplitude variation in the range of-481 to 336 nT in the study area due to wide variation of susceptibility values of various lithologic units (magnetic/moderate-magnetic basement). High amplitude, short wavelength anomaly pattern in the north-eastern and north-western part of the area shallow nature of the basement. Since the contact is unconformable, the boundary in magnetic anomaly image is gradational. The magnetic bodies are oriented in the NE-SW direction marked in the magnetic anomaly image. This is also evident in the hill shade image of the residual magnetic anomaly map.

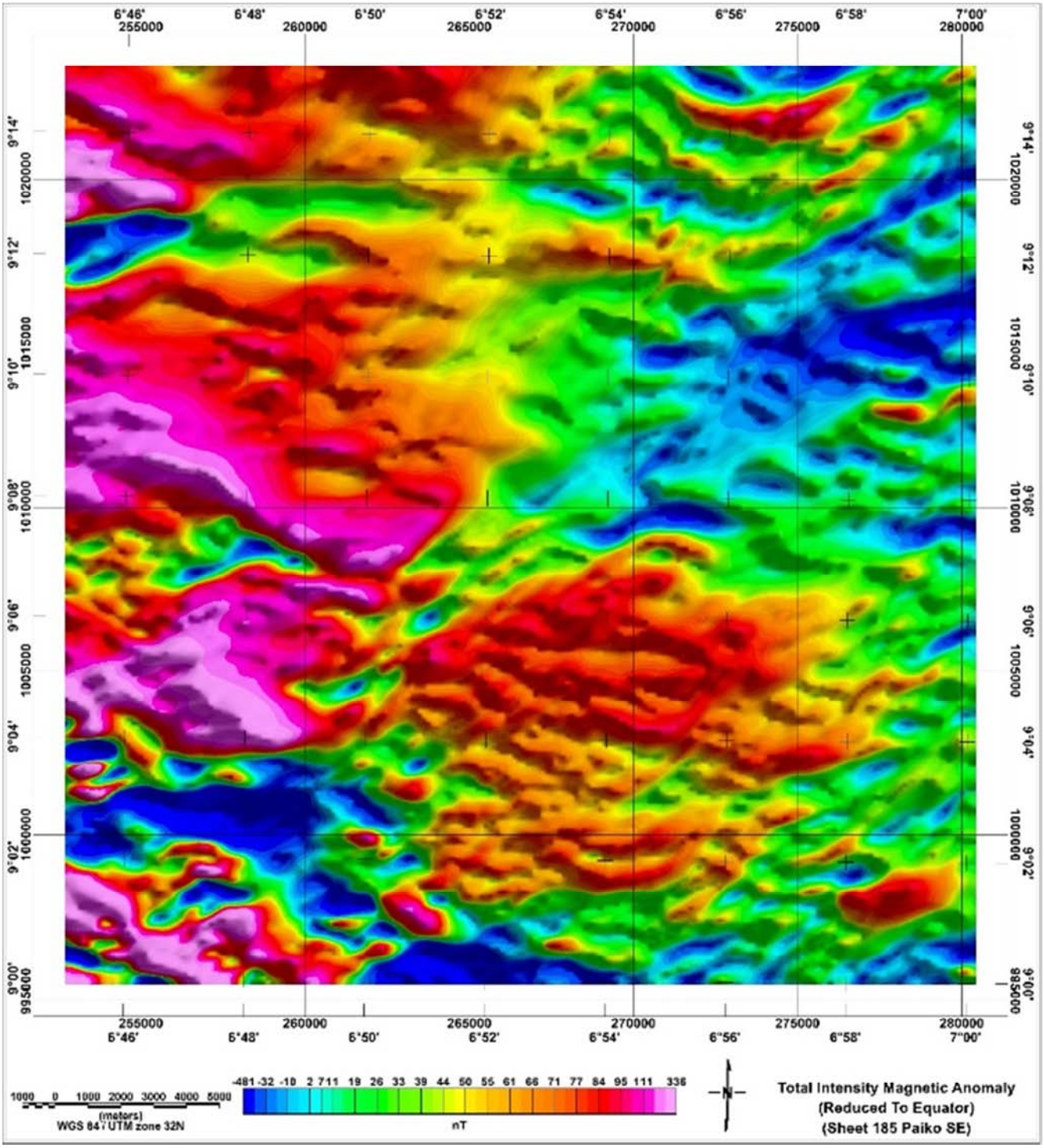

Figure 4. *Total Intensity Magnetic Anomaly map of Sheet 185 (Paiko SE). Areas in magenta are of high magnetic intensity, while blue coloured areas have low magnetic intensities. Data was processed using Oasis montaj software.*

Detailed structural fabric has been deciphered based on study of First vertical derivative image (Figure 5) and tilt derivative image (Figure 6). All zones of magnetic minima as well as displacements/discontinuities of magnetic anomalies were interpreted as linear structures. Some of these negative anomalies have remarkable positive anomalies at the edges, though not all of the structures are lined with these positive anomalies. The presence of linear, negative and positive anomalies next to each other is due to the general geometry of magnetic anomalies [57].

First vertical derivative image indicates that magnetic linears generally trend NE-SW sectors with minor NE-SW and E-W components. Basement faults are better resolved by linear structures along NE-SW directions are dominant with minor E-W and NW-SE components.

The amplitude of the signal peak of analytic signal (Figure 7) is directly proportional to the edge of magnetization. Hence, source edges are easily determined. The analytic signal has a form over causative body that depends on the locations of the body (horizontal coordinate and depth) but not on its magnetization direction. Analytic signal is often effective at highlighting geologically meaningful subtle anomalies [58]. Tilt Derivative revealed short wavelengths and enhanced the presence of magnetic lineaments as well as boundaries of magnetic bodies within the study area using its zero-crossing.

The radiometric response in the ternary map (Figure 8) to some extent corresponds with the surface rock units of the study area and shows a close spatial correlation with the rock units. The visual inspection of this map shows that high concentration of K, eTh and eU radioactive elements are displayed in lighter colour and related to Older Granites.

The composite image does not provide colour discrimination between older granites (OGp) and the (OGm). This can be discussed to the resemblance of radioelements content and the redistribution of radioelements concentration in the overburden because of high weathering process. There was however, a discrimination between the Migmatitic rocks (MG).

4.3. Fuzzy Integration

The fuzzy logic technique was used to construct a prospectivity mapping model for hydrothermal gold deposits and highlighted potential exploration targets in the study area. Evidential maps of the Landsat, Aster, derived aeromagnetic and radiometric maps were used for evaluating the importance of each data set in data analysis algorithm. The prospectivity map highlighted three potential exploration targets for gold mineralization within the study area. The predicted favourable zones coincide spatially with anomalous zones for stream sediment Au, Ag, Zn and Pb contents (Figure 9) and suggested for future detailed exploration.

5. Conclusion

Satellite imagery and aerogeophysical datasets were used to map hydrothermal alteration zones and extract the structural lineaments. Based on the exploration model considered for the study area, appropriate evidence maps include hydrothermal alteration, host rock and structural maps were developed, weighted and reclassified. Finally, fuzzy operators are applied to produce mineral prospectivity map. Mineral prospectivity map comparison with field studies revealed that the fuzzy logic model describes fairly well the favourability of the hydrothermal gold deposits in the study area. All produced maps in this study should be perceived as the preliminary evaluation of the study area in a reliable manner. The maps are a valuable data source for the detailed studies to be conducted in the future.

The results of remotely sensed images, aeromagnetic, aeroradiometric datasets and geology were integrated to produce a composite favourability map of the study area (Figure 9). The predominant tectonic trends are NE – SW, NW – SE and the E – W. The NE-SW (the predominant in the Basement Complex areas) was the most developed one among these trends and represents the preferred orientation of ore deposits. Also, a number of hydrothermally altered zones are mapped from the Landsat OLI and ASTER images. Since these zones have one or more structures associations, they serve as channel pathways for migrating hydrothermal fluids that contemporaneously reacts with rock formation which got altered subsequently. The alteration zones marked by low magnetic intensity and significant radiometric response lie within or close to a structure that has a NE – SW trend identified previously. The coincidence areas of these alteration zones and high complexity lineaments indicated a high possibility for the occurrence of gold mineralization in other similar locations. Thus, as mentioned previously, the close concordance between these known mineralization locations and the interpreted structural complexities sheds a light towards the similar mapped features that may be new promising sites. However, precise detection and evaluation of these ores need more geological and geophysical follow up survey with finer spacing.

As a consequence, the use of satellite images for hydrothermal alteration mapping and spatial data modelling during the early stages of mineral exploration has been found to be very successful in delineating the hydrothermally altered rocks. Conceptual fuzzy-logic method also gives a flexible tool to test exploration models in an easily understood manner for geologists. The uncertainties of the fuzzy-logic modelling could not be estimated easily, but an expert validation process would in many cases be appropriate and lead to reliable results.

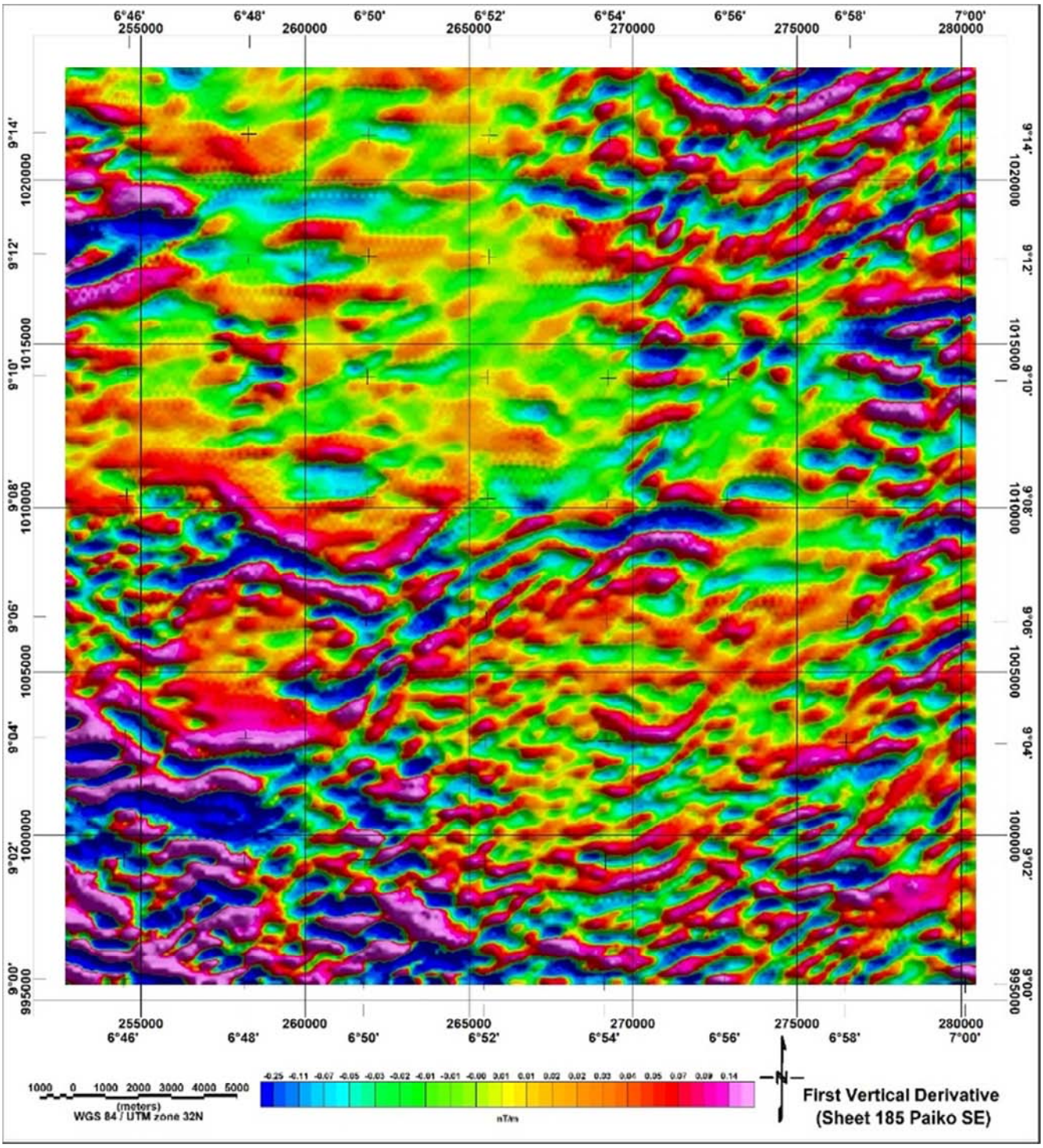

Figure 5. *First Vertical Derivative map of Sheet 185 (Paiko SE). Data was processed using Oasis montaj software.*

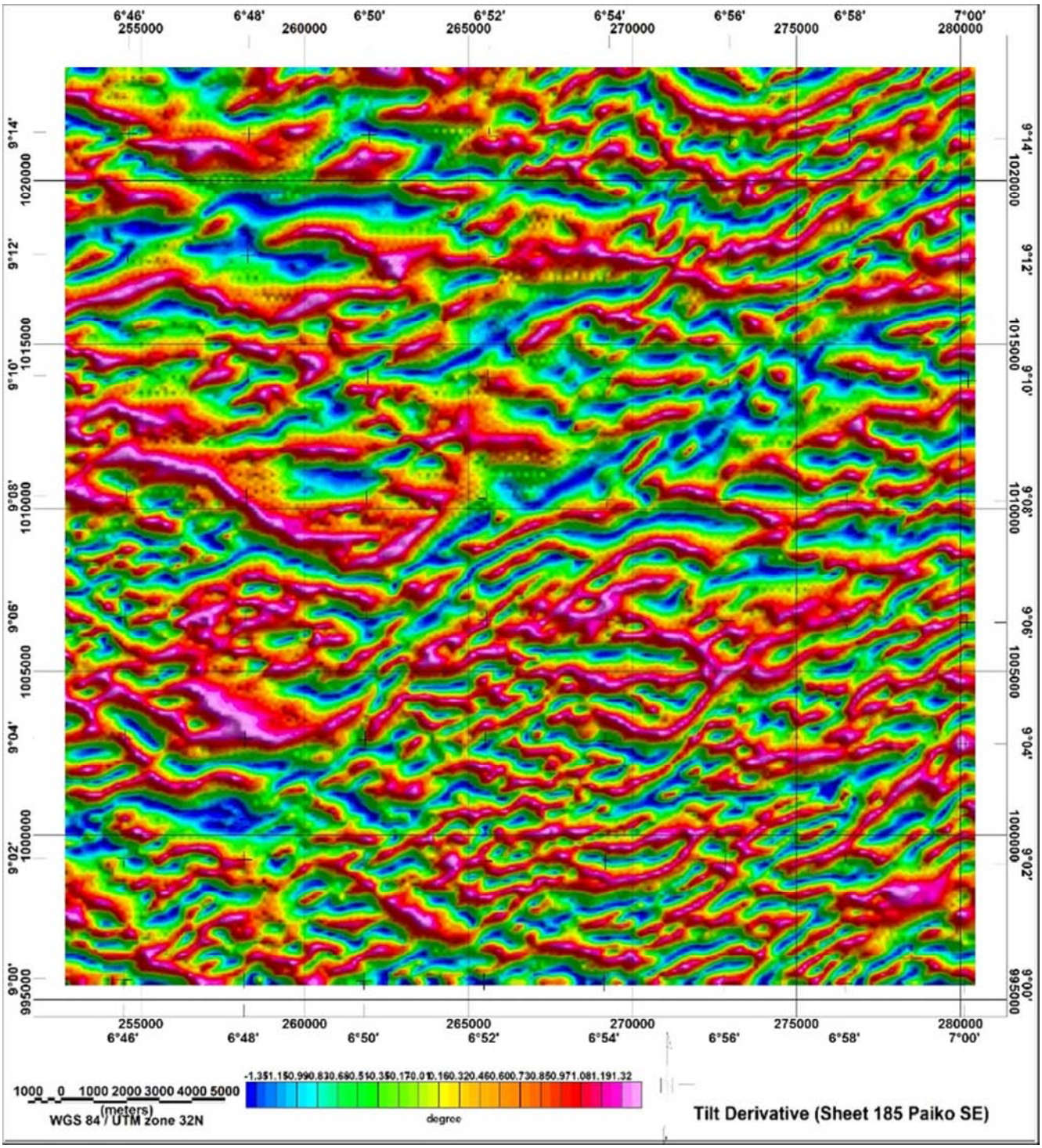

Figure 6. *Tilt Derivative map of Sheet 185 (Paiko SE). Data was processed using Oasis montaj software. Minima, represented by areas in blue, allowed for the delineation of magnetic lineaments.*

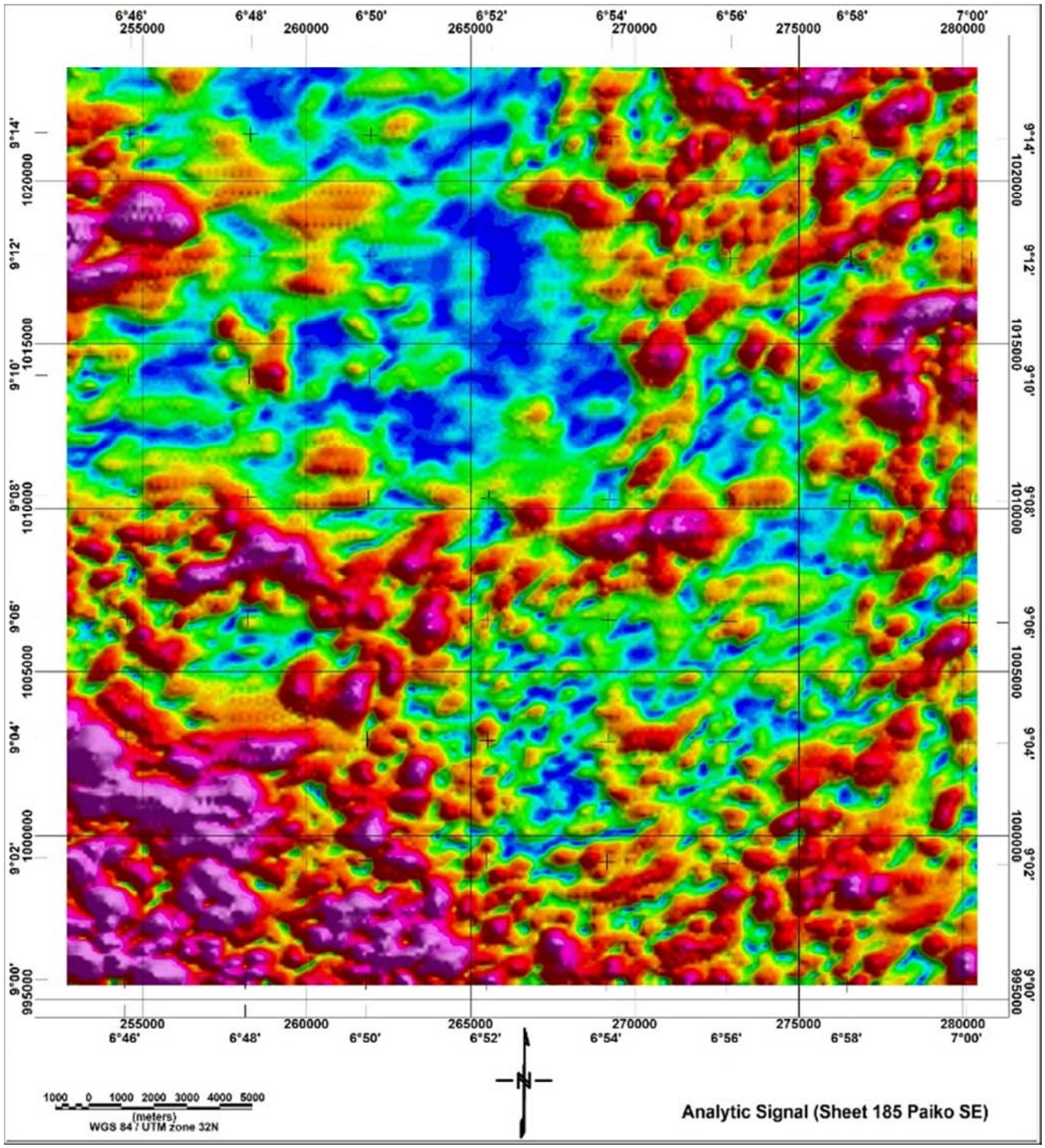

Figure 7. *Analytic Signal map of Sheet 185 (Paiko SE). Data was processed using Oasis montaj software. Maxima, represented by areas in magenta, show edge/contact of discreet bodies.*

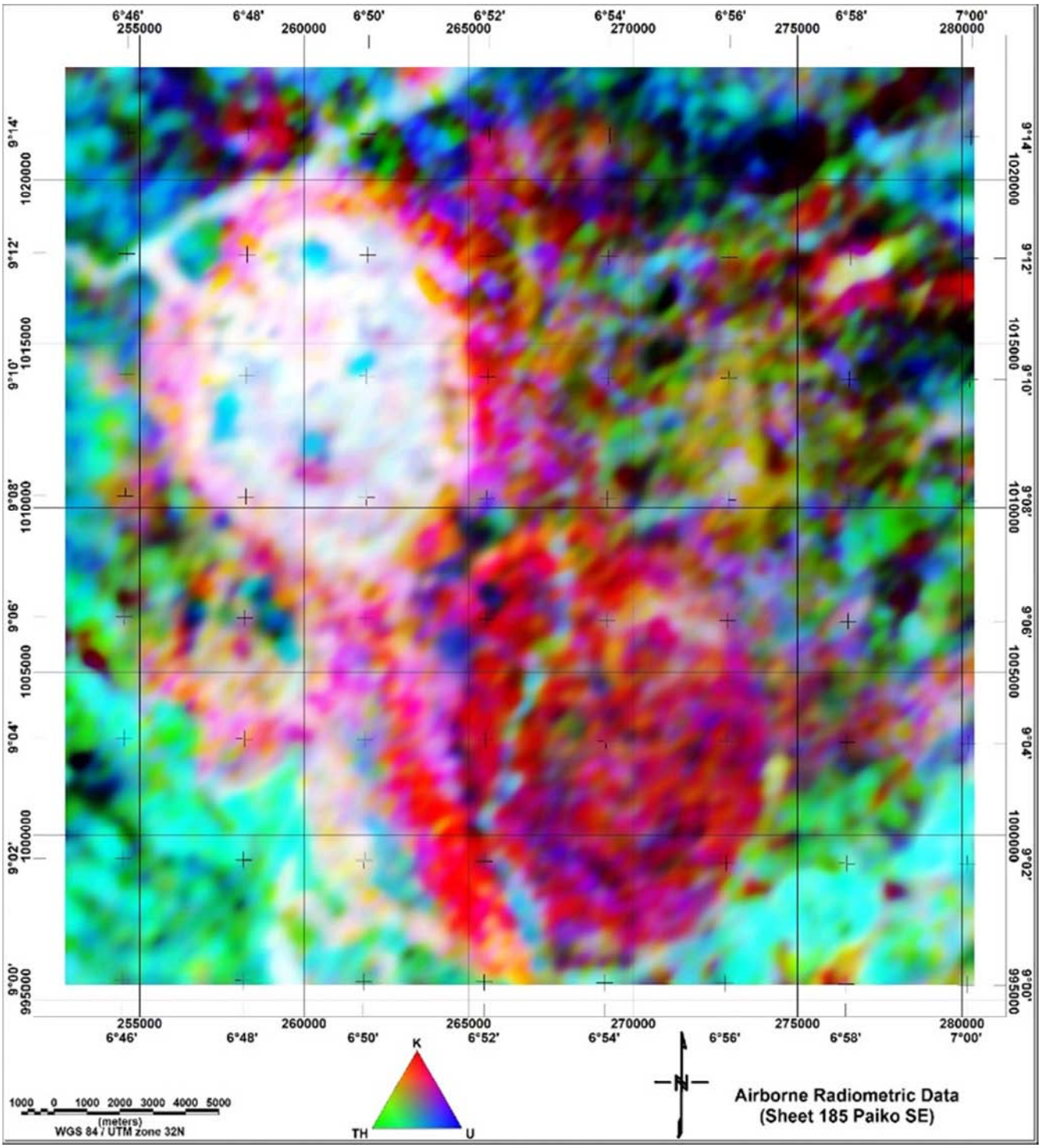

Figure 8. *Ternary Map of Sheet 185 (Paiko SE). Data was processed using Oasis montaj software. Areas in magenta represent zones of high K content. Areas in green represent zones of high Th content while areas in blue highlight areas enriched in U.*

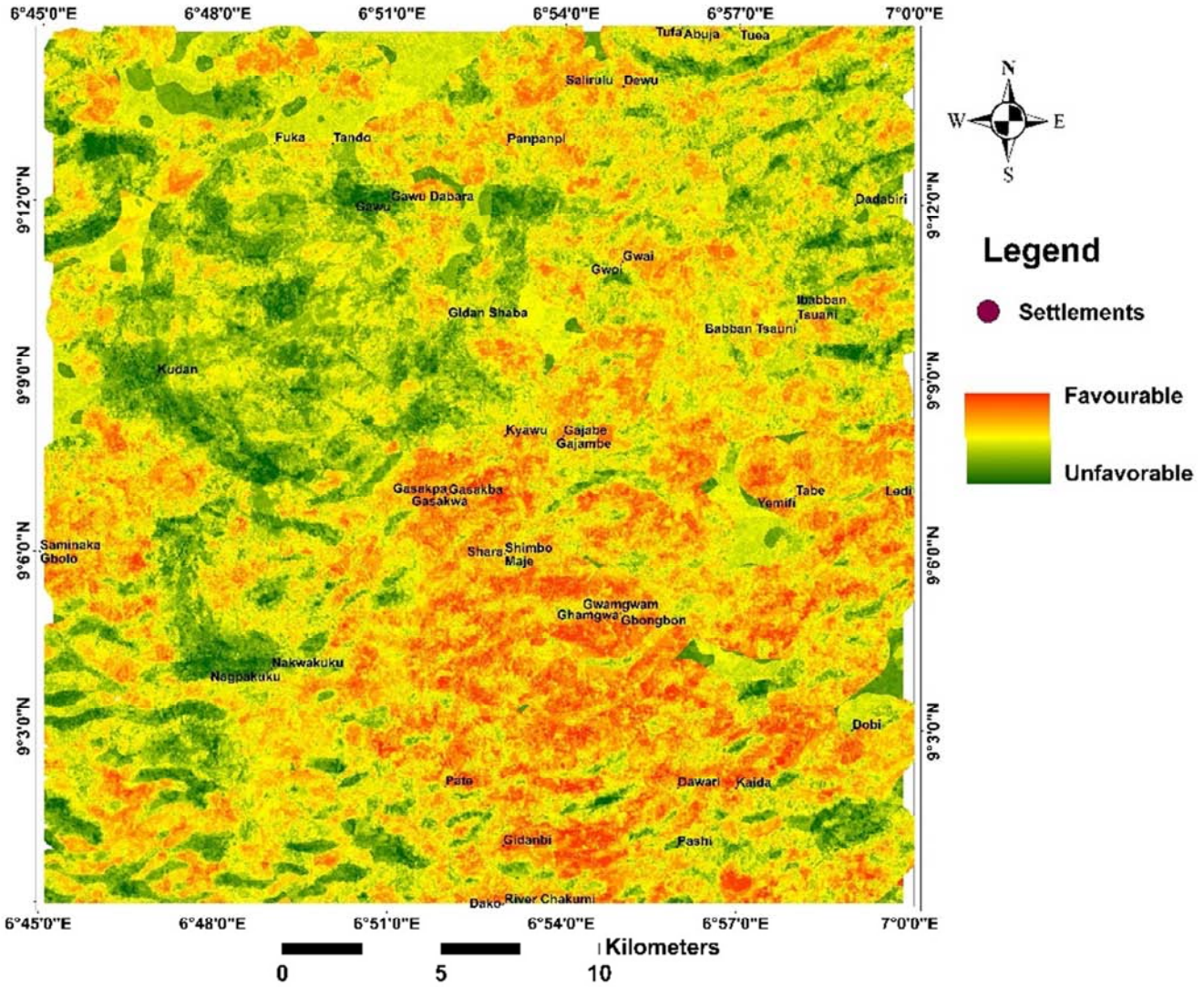

Figure 9. *Favourability map of Sheet 185 (Paiko SE). Areas in orange are delineated as areas more favourable to mineralisation. Green areas have been adjudged unfavourable.*

References

[1] Bonham-Carter, G. F. (1994). Geographic information systems for geoscientists: Modelling with GIS. Oxford: Pergamon Press.

[2] Yousefi, M., & Carranza, E. J. (2017). Union score and fuzzy logic mineral prospectivity mapping using discretized and continuous spatial evidence values. *Journal of African Earth Sciences, 128*, 47-60. doi: 10.1016/j.jafrearsci.2016.04.019.

[3] Nykänen V, Salmirinne H (2007). Prospectivity analysis of gold using regional geophysical and geochemical data from the Central Lapland Greenstone Belt, Finland. Gold in the Central Lapland Greenstone Belt: Geological Survey of Finland, Special Paper 44: 251–269.

[4] Behnia, P., Kerswill, J., Bonham-Carter, G., & Harris, J. (2009). Prospectivity mapping for gold deposits hosted by iron formation, in a portion of Western Churchill Province that includes Melville Peninsula, Nunavut, Canada. *2009 17th International Conference on Geoinformatics*. doi: 10.1109/geoinformatics.2009.5293437.

[5] Carranza EJM, Hale M (2001). Geologically-constrained fuzzy mapping of gold mineralization potential, Baguio district, Philippines. Nat Resour Res 10: 125–136.

[6] Masoud Moradi & Sedigheh Basiri & Ali Kananian & Keivan Kabiri (2014). Fuzzy logic modeling for hydrothermal gold mineralization mapping using geochemical, geological, ASTER imageries and other geo-data, a case study in Central Alborz, Iran. Earth Sci Inform DOI 10.1007/s12145-014-0151-9.

[7] Zhang, X., Pazner, M., and Duke N. (2007). Lithologic and mineral information extraction for gold exploration using ASTER data in the south Chocolate Mountains (California) ISPRS Journal of Photogrammetry & Remote Sensing 62 (2007) 271–282.

[8] Quadros TF, Koppe JC, Strieder AJ et al (2006). Mineral-potential mapping: a comparison of weights of evidence and fuzzy methods. Nat Resour Res 15: 49–65.

[9] Abubakar, A. J., Hashim, M., & Pour, A. B. (2018). Using ASTER Satellite Data for Mapping Hydrothermal Alteration as a Tool in Geothermal Exploration with GPS Field Validation. *Advanced Science Letters, 24* (6), 4489-4495. doi: 10.1166/asl.2018.11632.

[10] Ejepu J. S., Arikawe, E. A. and Abdullahi, S. (2018). Geological, Multispectral and Aeromagnetic Expressions of Pegmatite Hosted Mineralization of Keffi Sheet 208 NE, North-Central Nigeria. American Journal of Modern Physics and Application. Vol. 5, No. 4, pp. 53-69.

[11] Gabr, S. S., Hassan, S. M. and Sadek, M. F. (2015). Prospecting for new gold-bearing alteration zones at El-Hoteib area, South Eastern Desert, Egypt, using remote sensing data analysis. Ore Geology Reviews, Elsevier.

[12] Odeyemi, I. B. (1988). Lithostratigraghic and structural relationships of the upper Precambrian metasediments in Igarra area. In: Precambrian Geology of Nigeria. *Geological survey of Nigeria,* pp. 111-125.

[13] Rahaman, M. A. (1988). Recent advances in the study of the Basement Complex of Nigeria. Precambrian Geology of Nigeria, *Geological Survey of Nigeria Publications,* 11-43.

[14] Oyawoye, M. O. (1962). The Petrology of the District around Bauchi, Northern Nigeria. *The Journal of Geology, 70* (5), 604-615. doi: 10.1086/626855.

[15] Black, R. (1980). Precambrian of West Africa. *Episodes*, 4, 3–8.

[16] Ajibade, A. C., Woakes, M. & Rahaman, M. A. (1981). Proterozoic crustal development in the Pan-African regime of Nigeria. In Kroner, A. (Ed.), *Precambrian Plate Tectonics, Elsevier,* Amsterdam.

[17] Caby, R. Bertrand, J. M. I. and Black, R. (1981). Pan African ocean closure and continental collision in the Hoggar-Iforas segment, central Sahara. In: A Kroner (Editor) Precambrian plate tectonic. *Elsevier, Amsterdam*, 407-434.

[18] Dada, S. S. (2006). Proterozoic evolution of Nigeria. In Oshi O. (Eds.), *The Basement Complex of Nigeria and its Mineral Resources* (A tribute to Prof. M. A. Rahaman). (pp. 29-44). Akin Jinad and Co. Ibadan.

[19] Rahaman, M. A. & Ocan, D. (1978). On Relationship in the Precambrian Migmatite-gneiss on Nigeria. *Journal of Mining and Geology, 15,* 23-32.

[20] Grant, N. K. (1978). Structural distinction between a sedimentary cover and an underlying basement in 600 m.y. old Pan-African domain of northwestern Nigeria, West Africa. *Geological Society American Bulletin* 89: 50-58.

[21] McCurry, P. (1976). The geology of the Precambrian to Lower Palaeozoic rocks of northern Nig. A review In: C. A. Kogbe (Editor) geology of Nigeria. *Elizabethan press Lagos*, 15-39.

[22] Olade, M. A. and Elueze, A. A. (1979). Petrochemistry of Illesha Amphibolites and Precambrian Crustal Evolution in the Pan-African Domain of Southwestern Nigeria. Precambrian Research, 8, Pp. 308-318, 1979.

[23] Dada, S. S., Lancelot, J. R. and Briqueu, I. (1987). Age and origin of a Pan-African charnockitic complex: U-Pb and Rb-Sr evidence from the charnockitic complex at Toro, Northern Nigeria. Abtr. Vol. 14 Coll. Afri. Geol. Berlin, 72-73.

[24] Oluyide, P. O. (1988). Structural trends in the Nigerian Basement Complex. In: Precambrian Geology of Nigeria. *Geological Survey of Nigeria*, pp. 93-98.

[25] Olasehinde P. I. (1999). An integrated geologic and geophysical exploration technique for groundwater in the Basement Complex of West Central Nigeria. *Water Resources Journal*, 10, 46-49.

[26] Olasehinde P. I., Ejepu S. J. & Alabi A. A. (2013). Fracture Detection in a Hard Rock Terrain Using Radial Geoelectric Sounding Techniques. *Water Resources Journal* 23 (1&2), 1-19.

[27] Olasehinde, P. I. (2010). The Groundwaters of Nigeria: A Solution to Sustainable National Water Needs. *Federal University of Technology, Minna Inaugural Lecture Series 17*

[28] Gupta, R. P. (2003). Remote Sensing Geology, second ed. Springer-Verlag, Berlin.

[29] USGS/NASA (2015). Landsat 8 (L8) Data User's Handbook; USGS/NASA: Sioux Falls, SD, USA, p. 106.

[30] Abrams, M., Hook, S. (2001). ASTER User Handbook (version 2). Jet Propulsion Laboratory, Pasadena, CA-91109, USA. 135 pp.

[31] Crósta, A. P., Filho, C. R. d. S. (2003). Searching for gold with ASTER. Earth Observation Magazine 12 (5), 38–41.

[32] Ninomiya, Y., Fu, B., Cudhy, T. J. (2005). Detecting lithology with Advanced Spaceborne Thermal Emission and Refection Radiometer (ASTER) multispectral thermal infrared "radiance-at-senseor" data. Remote Sensing of Environment 99, 127–135.

[33] Ninomiya, Y., Fu, B., Cudhy, T. J. (2006). Corrigendum to "Detecting lithology with Advanced Spaceborne Thermal Emission and Refection Radiometer (ASTER) multispectral thermal infrared 'radiance-at-sensor' data". Remote Sensing of Environment 101, 567.

[34] Gad, S., Kusky, T. (2006). Lithological mapping in the Eastern Desert of Egypt, the Barramiya area, using Landsat thematic mapper (TM). Journal of African Earth Sciences 44, 196–202.

[35] Gad, S., Kusky, T. (2007). ASTER spectral ratioing for lithological mapping in the Arabian Nubian shield, the Neoproterozoic Wadi Kid area, Sinai, Egypt. Gondwana Research 11, 326–335.

[36] International Geomagnetic Reference Field-11th Generation (2009). https://www.ngdc.noaa.gov/metaview/page?xml=NOAA/NESDIS/NGDC/MGG/GeophysicalModels/iso/xml/IGRF11.xml&view=getDataView&header=none.

[37] Briggs IC (1974). Machine contouring using minimum curvature. Geophysics 39 (1): 39-48.

[38] Crippen, R. E., E. J. Hajic, J. E. Estes, and R. G. Blom (1990). Statistical band and band-ratio selection to maximize spectral information in color composite displays, in preparation for submission to international Journal of Remote Sensing.

[39] Zhang, X.; Pazner, M. Comparison of Lithologic Mapping with ASTER, Hyperion and ETM Data in the Southeastern Chocolate Mountains, USA. Photogramm. Eng. Remote Sens. 2007, 73, 555–561.

[40] Ninomiya, Y. (2003). A stabilized vegetation index and several mineralogic indices defined for ASTER VNIR and SWIR data. Proceedings of IEEE 2003 International Geoscience and Remote Sensing Symposium: IGARSS'03, 3, pp. 1552–1554.

[41] Nabighian, N. N. (1984). Towards a Three-dimensional Automatic Interpretation of Potential Field Data via Generalized Hilbert Transforms: Fundamental Relations, Geophysics49, 780–786.

[42] Ansari, A.H. and Alamdar, K. (2009) Reduction to the Pole of Magnetic Anomalies Using Analytic Signal. World Applied Sciences Journal, 7, 405-409.

[43] Roest, W. R., Verhoef, J., Pilkington, M. (1992). Magnetic interpretation using 3-D analytic signal. Geophysics 57, 116–125.

[44] Ostrovskiy, E. (1975). Antagonism of radioactive elements in wallrock alterations fields and its use in aerogamma spectrometric prospecting. *International Geology Review, 17* (4), 461-468. doi: 10.1080/00206817509471687.

[45] Lillesand, T. M., Kiefer, R. W. (2004). Remote Sensing and Image Interpretation, fifth ed. John Wiley and Sons, Inc., New York.

[46] Schowengerdt, R. A. (2007). Remote Sensing: Models and Methods for Image Processing, 3rd ed., Academic Press, London.

[47] Gupta, R. (2016). Enhanced Edge Detection Technique for Satellite Images. *Cloud Computing and Security Lecture Notes in Computer Science,* 273-283. doi: 10.1007/978-3-319-48671-0_25.

[48] Batista, C. T., Veríssimo, C. U. V., Amaral, W. S. (2014). Levantamento de feições estruturais lineares a partir de sensoriamento remoto – uma contribuição para o mapeamento geotécnico na Serra de Baturité, Ceará. Geologia USP. Série Científica, 14 (2), 67-82. http://dx.doi.org/10.5327/Z1519-874X201400020004.

[49] Kovesi, P. (1997). Symmetry and Asymmetry from Local Phase, in: Tenth Australian Joint 593 Converence on Artificial Intelligence. pp. 2–4. 594.

[50] Kovesi, P. (1999). Image Features from Phase Congruency. The MIT Press, Videre: Journal of 595 Computer Vision Research Volume 1, 1–26.

[51] Boleneus DE, Raines G, Causey J *et al.,* (2001) Assessment method for epithermal gold deposits in northeast Washington State using weights-of-evidence GIS modeling. US Department of the Interior, US Geological Survey, Menlo Park.

[52] Sabins, F. (1997). Remote Sensing: Principles and interpretation (2nd ed.). NY: Freeman.

[53] Knepper, D. H., Jr., (1989). Mapping hydrothermal alteration with Landsat Thematic Mapper data, Lee, Keenan, ed., Remote sensing in exploration geology — A combined short course and field trip: 28th International Geological Congress Guidebook T182, p. 13–21.

[54] Khalid A., Elsayed Z. and AbdelHalim H. (2014). The Use of Landsat 8 OLI Image for the Delineation of Gossanic Ridges in the Red Sea Hills of NE Sudan. *American Journal of Earth Sciences*. Vol. 1, No. 3. pp. 62-67.

[55] Pour, A. B., Hashim, M. & Marghany, M. (2014). Exploration of gold mineralization in a tropical region using Earth Observing-1 (EO1) and JERS-1 SAR data: a case study from Bau gold field, Sarawak, Malaysia. Arab J Geosci 7: 2393. https://doi.org/10.1007/s12517-013-0969-3.

[56] Ducart, D. F., Crosta, A. P., Filho, C. R., & Coniglio, J. (2006). Alteration Mineralogy at the Cerro La Mina Epithermal Prospect, Patagonia, Argentina: Field Mapping, Short-Wave Infrared Spectroscopy, and ASTER Images. *Economic Geology, 101* (5), 981-996. doi: 10.2113/gsecongeo.101.5.981.

[57] Telford W. M., Geldart, L. P. & Sheriff, R. E. (1990). Applied geophysics, Cambridge University Press.

[58] Lyatsky, H.V. (2004): The meaning of anomaly; Recorder, Canadian Society of Exploration Geophysicists, v. 29, no. 6, p. 50-51.

[59] Ostrovskiy, E. A. (1975). Antagonism of radioactive elements in wallrock alteration fields and its use in aerogamma spectrometric prospecting. Int. Geol. Rev. 17 (4), 461–468.